frontiers | Frontiers in Materials

TYPE Original Research
PUBLISHED 02 December 2022
DOI 10.3389/fmats.2022.1055641

OPEN ACCESS

EDITED AND REVIEWED BY
Derun Zhang,
Huazhong University of Science and Technology, China
Tingting Huang,
Wuhan University of Technology, China
Zhe Zeng,
North Carolina State University, United States

*CORRESPONDENCE
Chen Jiangcai,
jiangcai_hit@163.com

SPECIALTY SECTION
This article was submitted to Structural Materials, a section of the journal Frontiers in Materials

RECEIVED 28 September 2022
ACCEPTED 26 October 2022
PUBLISHED 02 December 2022

CITATION
Jiangcai C, Zhiwei L, Zihong Z, Xiaofeng H, Jie C and Zhiyang L (2022), Investigation on temperature shrinkage characteristics of the combined structure in asphalt pavement. *Front. Mater.* 9:1055641. doi: 10.3389/fmats.2022.1055641

Investigation on temperature shrinkage characteristics of the combined structure in asphalt pavement

Chen Jiangcai[1]*, Li Zhiwei[2], Zhao Zihong[3], Huang Xiaofeng[1], Chen Jie[1] and Liu Zhiyang[4]

[1]Guangxi Beitou Transportation Maintenance Technology Group CO LTD, Nanning, Chia, [2]School of Transportation Science and Technology, Harbin Institute of Technology, Harbin, China, [3]Guangxi Communications Design Group CO LTD, Nanning, China, [4]College of Civil and Transportation Engineering, Shenzhen University, Shenzhen, China

The temperature shrinkage of materials primarily causes transverse cracking. Current research mainly focuses on the temperature shrinkage of single materials. This work aims to analyze the effect of the structural combination on temperature shrinkage. To this end, the temperature rise method was first discussed to measure the shrinkage coefficient to replace the traditional temperature drop method. Then, the temperature shrinkage coefficients of the lime–fly ash-stabilized macadam, and ATB and AC asphalt mixtures were measured. The effect of gradation types, lime–fly ash content, and nominal maximum aggregate size on the temperature shrinkage was studied. Finally, the temperature shrinkage of composite structural characteristics was analyzed. The results show that the difference between the temperature shrinkage coefficients obtained by temperature rise and drop methods was relatively small. Thus, the temperature rise method can be used to measure the temperature shrinkage coefficient. In addition, the lime–fly ash-stabilized macadam with the suspended dense gradation or a higher lime–fly ash content has the largest temperature shrinkage strain. The suspended dense gradation should be avoided, and the content of lime–fly ash should be approximately reduced to control the temperature shrinkage strain of the semi-rigid base course. As for the asphalt mixture, the temperature shrinkage strain increased with the decrease in the nominal maximum aggregate size. The asphalt mixture with a larger nominal maximum aggregate size should be given priority to control the temperature shrinkage. Finally, when combined with the base course or surface layer, the temperature shrinkage of the base course was promoted by the surface layer, while the base course inhibited the surface layer. Meanwhile, the mutual influence between the semi-rigid base course and the surface layer was more substantial than that of the mutual influence between the flexible base course and surface layer.

KEYWORDS

asphalt pavement, semi-rigid base, surface layer, composite structure, temperature shrinkage coefficient

1 Introduction

The transverse crack is one of the typical damage forms in asphalt pavement that significantly reduces the pavement performance and shortens its service life (Boucart et al., 2005; Zang et al., 2018; Ma et al., 2019). Transverse cracks are primarily caused by temperature and base reflection. Meanwhile, under low temperatures, the flexible base can quickly produce temperature shrinkage due to its high-temperature sensitivity, accumulating shrinkage stress (Yang et al., 2013; Wang et al., 2018; Zhai et al., 2018). When the stress exceeds its tensile strength, the material cracks easily. In China, the semi-rigid and flexible bases are the main forms of the pavement structure (Zhai et al., 2021). Therefore, this study examines how to control or evaluate temperature shrinkage deformation.

Typically, temperature shrinkage tests start at high temperatures and gradually cool down by a temperature control program to measure the specimen's shrinkage (Chu et al., 2012; Ma et al., 2013; Li et al., 2017). This method, however, is more complex and requires more sophisticated equipment. Research has shown that heating can replace cooling to measure shrinkage coefficients. Yang (2004) demonstrated that the lime–fly ash-stabilized macadam has similar shrinkage and expansion laws in dry conditions. Despite a slight difference, the shrinkage and expansion coefficients at different temperatures are similar. As a result, Tian (2010) compared the shrinkage and expansion laws of a cement-stabilized macadam material in different temperature conditions, finding that the material's shrinkage and expansion characteristics remained the same for both temperature increases and decreases.

The temperature shrinkage test of semi-rigid base mixtures has been studied extensively. In the study of asphalt pavement failure forms, Coetzee et al. (1979) examined the stress distribution around the pavement crack under the action of temperature and the driving load based on the effective stress and concluded that the displacement in the vertical and horizontal directions is the cause of the reflection crack of the pavement after the base layer cracks. Hernando et al. (2016) found that shrinkage cracking, reflection cracking, and temperature fatigue cracking are the leading causes of transverse cracking. Szwed et al. (2015) developed an analytical model for preventing low-temperature cracking of asphalt pavement and also gave the maximum elastic modulus for different depths of asphalt pavement for the cooling process. Based on fatigue testing of various asphalt pavement materials, Fallah et al. (2015) found that reflection cracks expand between 10^{-4} and 10^{-5}mm/time. Kazimierowicz et al. (2016) conducted numerical simulations to investigate the effects of cracking on semi-rigid pavements. The results show that even a monomer crack in the base will significantly reduce the pavement service life. Akentuna et al. (2016) developed a device for measuring the temperature stress of the asphalt mixture and found through experimental research that the grade and content of the binder in the asphalt mixture, void ratio, and shrinkage coefficient of the aggregate and mixture have essential effects on the temperature stress of the asphalt mixture. Briefly, most existing studies focus on the grading composition of the semi-rigid base mixture, the amount of cementitious material, and the curing age, while a few studies are conducted using additives to improve the early strength of the mixture. Although the research angles are different, the aforementioned research mainly focuses on the semi-rigid base without considering how the surface course impacts the base shrinkage. Meanwhile, most studies on the asphalt-stabilized macadam are conducted from a mixture grading perspective.

This study aims to analyze the effect of the structural combination on the temperature shrinkage characteristic. To this end, the temperature rise method was first discussed to measure the temperature shrinkage coefficient. Then, temperature shrinkage coefficients of the lime–fly ash-stabilized macadam, and ATB and AC asphalt mixtures were measured. Also, factors affecting temperature shrinkage were discussed. Furthermore, the temperature shrinkage characteristic of composite structures was analyzed. This study can provide a reference for the crack resistance design in asphalt pavement with semi-rigid bases.

2 Materials and methods

2.1 Materials

In this study, the aggregate used is from the construction section of the Hegang–Dalian expressway, the lime is supplied by Jilin Chemical Industry Company, and the fly ash is Class I fly ash from the Harbin Power Plant. The asphalt is 90# road petroleum asphalt, and its various performance indicators meet the requirements of the specification (JTG F40-2004 Standard test, 2004).

2.2 Specimen preparation

The lime–fly ash-stabilized macadam was used as the semi-rigid base material. Three typical base gradation types were selected, namely, suspension dense gradation (xm), framework pore gradation (gk), and dense framework gradation (gm). The ratio of lime to fly ash was 1:3. The contents of lime–fly ash were 15%, 17%, and 20%. The maximum dry density and optimum moisture content of the lime–fly ash-stabilized macadam in different gradations are listed in Table 1. The sample size was 100 mm × 100 mm × 400 mm (JTG E51-2009 standard;JTG E51-2009 standard). The sample was molded by vibration compaction, according to the standard method (JTJ 034-2000 Standard Test;JTJ 034-2000 Standard Test). Three parallel tests were performed on each mixture.

TABLE 1 Results of the maximum dry density and optimum moisture content.

Material type	15 xm	15 gk	15 gm	17 xm	17 gk	17 gm	20 xm	20 gk	20 gm
Maximum dry density (g/cm^3)	2.23	2.32	2.38	2.24	2.33	2.27	2.27	2.28	2.30
Optimum moisture content (%)	6.06	5.77	5.87	6.99	5.55	6.04	7.13	6.00	6.36

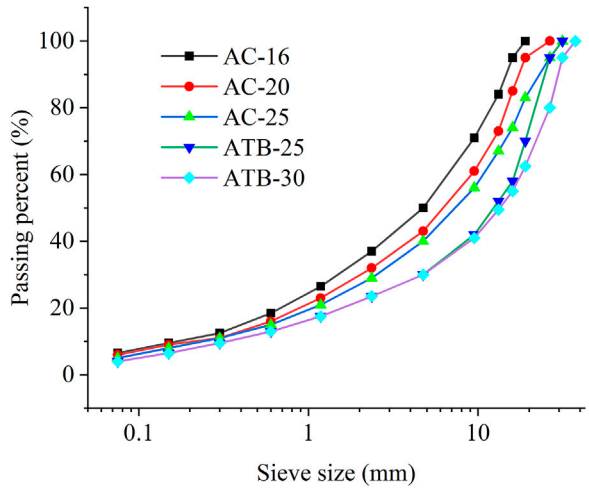

FIGURE 1
Gradation curves of the asphalt mixture.

The base layer is directly bonded to the subsurface layer in the pavement structure. Two dense-graded asphalt mixtures were adopted, namely, the dense asphalt mixture (AC) and dense asphalt-stabilized macadam mixture (ATB). The asphalt mixture is named by the grading type combined with the nominal maximum aggregate size. AC-16, AC-20, and AC-25 were used as surface course materials. Meanwhile, ATB-25 and ATB-30 were used as flexible base materials. The gradation curves of five types of asphalt mixtures are shown in Figure 1, and the optimum asphalt contents for AC-16, AC-20, AC-25, ATB-25, and ATB-30 were 4.53%, 4.3%, 3.9%, 3.47%, and 3.25%, respectively. The sample size of the flexible asphalt base was 100 mm × 100 mm × 400 mm. The sample size of the surface course was 60 mm × 100 mm × 400 mm. The samples were compacted by vibration.

2.3 Temperature shrinkage of materials

The temperature shrinkage coefficient was measured by gradually decreasing the temperature. However, this method was complicated and required sophisticated test instruments. Yang calculated the temperature shrinkage coefficient of the lime–fly ash-stabilized macadam in dry conditions. The results show that the lime–fly ash-stabilized macadam exhibited similar shrinkage characteristics during the heating and cooling processes, and the difference between shrinkage and expansion coefficients is slight. Tian et al. (1987) compared the shrinkage characteristic of the cement-stabilized macadam and asserted that the shrinkage and expansion coefficients were essentially the same. Therefore, this work first discussed the temperature rise method to measure the temperature shrinkage coefficient of the lime–fly ash-stabilized macadam and asphalt mixture.

A temperature sensor was embedded inside the specimen. The shrinkage deformation was measured by using a dial indicator with an accuracy of 10^{-3}mm. The specimen was first dried and cooled down to room temperature. A glass sheet was pasted on the specimen. Then, the specimen was kept in a low-temperature freezer for 3 h at −30°C. After removing from the freezer, the specimen was placed on the metal support. The value of the dial indicator and the temperature of the specimen were collected every 5 min in the first 2 h. After 2 h, the values were collected every 60 min until the value and temperature were basically unchanged. The test setup of the lime–fly ash-stabilized macadam, ATB mixture, and AC mixture is exhibited in Figure 2. The procedure of the temperature drop method was similar to that of the temperature rise method. The temperature shall be reduced step-by-step from high temperature, and the corresponding shrinkage of the specimen was measured. The temperature shrinkage strain and temperature shrinkage coefficient calculation formulae are as follows:

$$\varepsilon_i = \frac{\Delta l}{L_0}, \tag{1}$$

$$\alpha_t = \frac{\varepsilon_i}{\Delta t}, \tag{2}$$

where ε_i is the shrinkage strain at the i temperature (%), Δl is the temperature shrinkage deformation, L_0 is the initial length of the test specimen, α_t is the temperature shrinkage coefficient, and Δt is the temperature range (°C).

As the asphalt mixture surface layer and base formed a composite structure, they influence each other. Therefore, the shrinkage coefficient of composite structures should be measured. In order to closely bond the surface layer and base, SBS-modified asphalt was used as the binder and the coating thickness is approximately 1 mm (Feng, et al., 2007; Yu, et al., 2016). After bonding, heavy static pressure is applied on the top of the composite structure to strengthen the bond. The dial indicator was set at the bottom of the base course (A), at the bonding site (B), and at the top of the surface layer (C) (Figure 3).

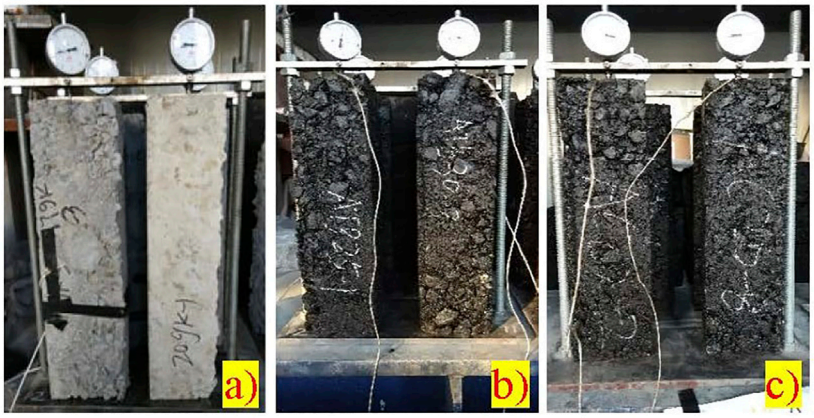

FIGURE 2
(A) Lime–fly ash-stabilized macadam; **(B)** ATB mixture; and **(C)** AC mixture.

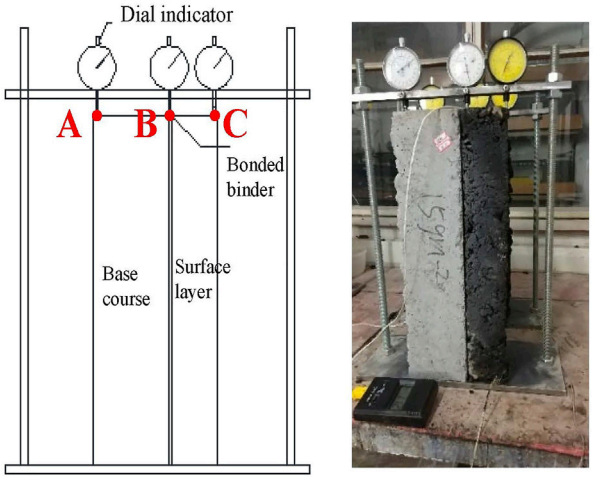

FIGURE 3
Composite structure.

3 Results and discussion

3.1 Comparison of the temperature shrinkage coefficient between the temperature rise and drop

As the shrinkage of the metal support (the temperature shrinkage coefficient is 12.1 × 10^{-6}/°C) affects the final results, it should be deducted when calculating the final results. The temperature shrinkage coefficient results of the lime–fly ash-stabilized macadam in different temperature ranges are listed in Table 1. It is noticeable from Table 2 that for the lime–fly ash-stabilized macadam, the shrinkage coefficients measured by the temperature rise method are smaller than those by the temperature drop method. For safety reasons, the temperature shrinkage coefficient measured by the temperature rise method needs to be adjusted. After comparison and analysis, the adjustment coefficient is determined to be 1.1.

It is found from Table 2 that for the same material, the temperature shrinkage coefficients measured by the temperature rise method and the temperature drop method in the same temperature range were not significantly different. The average temperature coefficients in different temperature ranges were almost the same, indicating that the temperature shrinkage and expansion laws of the lime–fly ash-stabilized macadam were similar in temperature rise and drop conditions. In addition, the temperature rise method can eliminate the influence of metal support during the temperature drop process. Therefore, the temperature rise method can be used to measure the temperature shrinkage coefficient for the lime–fly ash-stabilized macadam.

Table 3 shows that for AC and ATB asphalt mixtures, the temperature shrinkage and expansion laws were similar in temperature rise and drop conditions. The average temperature shrinkage coefficients measured by the temperature rise and drop methods were not significantly different. Therefore, the temperature rise method could be used to measure the temperature shrinkage coefficient for the asphalt mixture.

3.2 Temperature shrinkage coefficient of single pavement material

3.1.1 Lime–fly ash-stabilized macadam

The internal temperature of the lime–fly ash-stabilized macadam varies with time exhibits, as shown in Figure 4. It is

10.3389/fmats.2022.1055641

TABLE 2 Temperature shrinkage coefficient of the lime–fly ash-stabilized macadam in different temperature ranges.

Test method	Temperature range/°C	15 gm	15 xm	15 gk	17 gm	17 xm	17 gk	20 gm	20 xm	20 gk
Heating	−30~F02D20	6.25	5.67	7.92	8.08	8.37	6.40	9.17	11.08	11.17
	−20~F02D10	4.58	4.83	4.08	4.92	8.08	6.08	8.58	9.83	8.00
	−10 to 0	3.92	3.50	3.08	4.17	5.83	4.42	6.50	6.33	5.83
	0–10	3.92	4.33	2.4222	5.25	4.58	5.25	4.00	4.67	4.00
	10–18	6.56	11.46	5.83	9.69	7.71	8.02	6.04	6.56	3.75
	Average	5.05	5.96	4.67	6.42	6.92	6.03	6.86	7.70	6.55
	CV	25.3%	53.3%	47.7%	36.6%	23.7%	22.4%	30.3%	34.6%	47.2%
Cooling	−30~F02D20	6.33	7.50	4.58	6.58	8.08	6.67	7.75	8.92	7.25
	−20~F02D10	4.83	4.58	4.17	5.92	5.67	5.67	6.42	6.75	6.42
	−10 to 0	4.67	5.00	3.92	5.75	6.00	5.17	5.83	6.00	6.58
	0–10	4.83	4.50	4.25	5.58	6.83	6.75	5.08	6.67	5.42
	10–18	5.65	10.23	7.10	9.19	10.44	7.52	10.23	11.48	8.56
	Average	5.26	6.36	4.80	6.60	7.40	6.35	7.06	7.96	6.85
	CV	13.5%	39.1%	27.2%	22.6%	26.1%	14.7%	28.6%	28.3%	17.0%
Difference		−4.1%	−6.4%	−2.9%	−2.8%	−6.6%	−5.0%	−2.9%	−3.3%	−4.3%
Correction results		5.55	6.55	5.13	7.06	7.61	6.64	7.54	8.47	7.20

TABLE 3 Temperature shrinkage coefficient of the asphalt mixture in different temperature ranges.

Test method	Temperature range/°C	AC-16	AC-20	AC-25	ATB-25	ATB-30
Heating up	−30~F02D20	16.67	19.75	9.75	14.33	15.58
	−20~F02D10	19.75	11.58	11.67	12.58	11.08
	−10 to 0	34.17	24.42	30.00	20.92	18.50
	0–10	30.75	28.00	26.42	18.25	15.92
	10–18	41.25	43.02	27.92	21.88	18.85
	Average	28.52	25.35	21.15	17.59	15.99
	CV	35.8%	45.9%	45.6%	23.0%	19.5%
Cooling	−30~−20	23.33	18.00	14.92	13.67	15.33
	−20~−10	30.58	21.50	19.67	18.25	10.75
	−10 to 0	28.50	23.92	21.00	16.42	12.33
	0–10	28.25	27.83	22.08	13.58	13.83
	10–18	29.08	31.38	22.73	21.79	21.90
	Average	27.95	24.53	20.08	16.74	14.83
	CV	9.8%	21.4%	15.5%	20.5%	29.0%
Difference		2.0%	3.4%	5.3%	5.1%	7.8%
Correction results		27.95	24.85	20.73	17.24	15.67

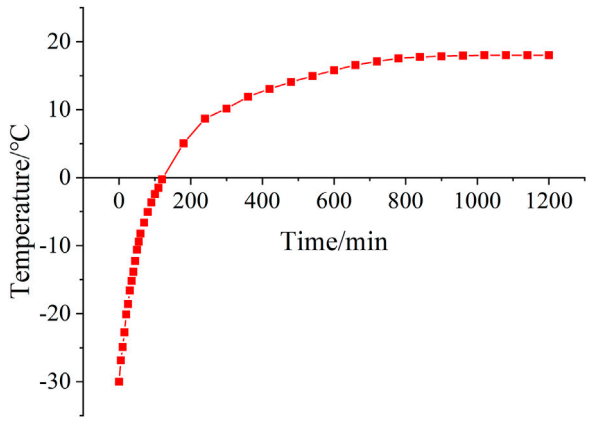

FIGURE 4
Relationship between the internal temperature and time of the lime–fly ash-stabilized macadam.

evident from Figure 4 that the internal temperature of lime–fly ash-stabilized macadam increased with the increase in time. When the time was in the first 180°min (temperature was less than 5°C), the internal temperature of the lime–fly ash-stabilized macadam increased sharply and then increased slowly with time. For example, when the time-increasing amplitude increased from 0 min to 180 min, the internal temperature of the lime–fly ash-stabilized macadam increased from −30°C to 5°C. However, when the time increased from 180°min to 1,000°min, the internal temperature only increased up to 18°C (temperature amplification is 13°C).

The temperature shrinkage strain of the lime–fly ash-stabilized macadam was affected by the gradation type. The influence of the gradation type on the temperature shrinkage strain in different lime–fly ash contents was analyzed. The lime–fly ash contents were 15%, 17%, and 20%. The time ranged from 0°min to 1,200°min. The variations of the temperature shrinkage strain of different gradation types with time are shown in Figure 5.

It is evident from Figure 5 that when the time increased from 0°min to 180°min, the temperature shrinkage strain increased sharply. For example, when the time-increasing amplitude increased from 0°min to 180°min, the temperature shrinkage strain of 15 xm increased from 0 to 1.59×10^{-4}. However, when the time increased to 1,000°min, the temperature shrinkage strain was 2.75×10^{-4}, and the growth rate was about one-sixth of the first

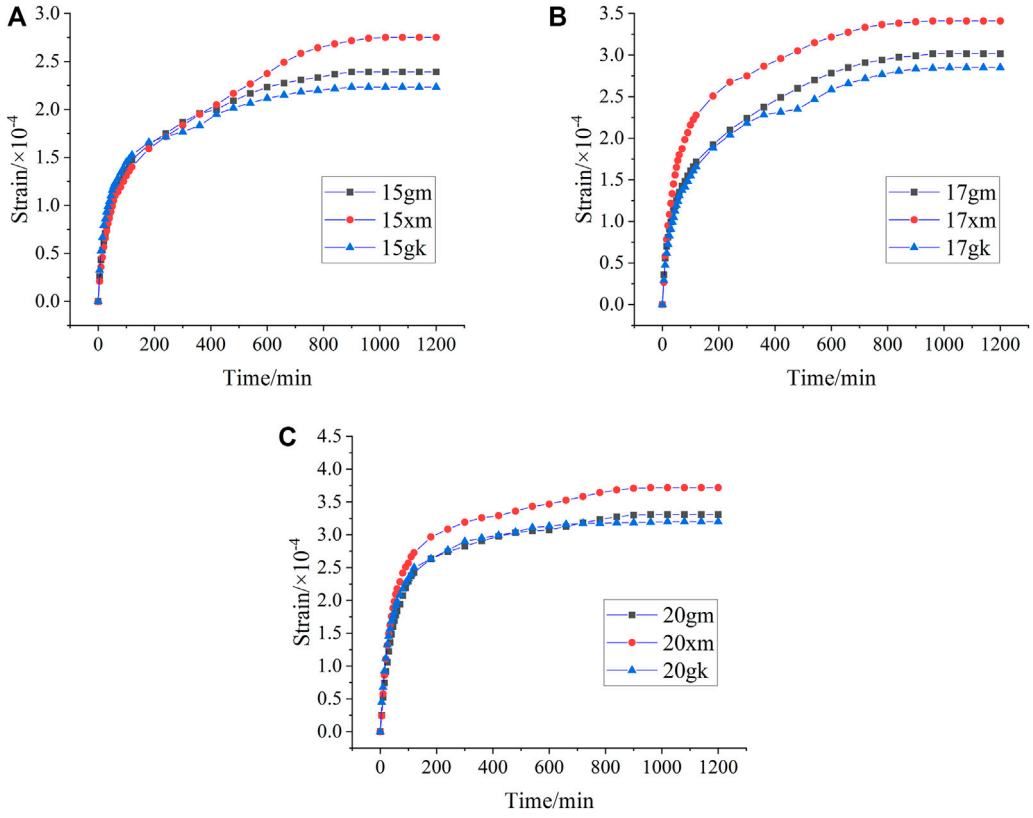

FIGURE 5
Relationship between the temperature shrinkage strain and time (lime–fly ash content unchanged): **(A)** 15%; **(B)** 17%; and **(C)** 20%.

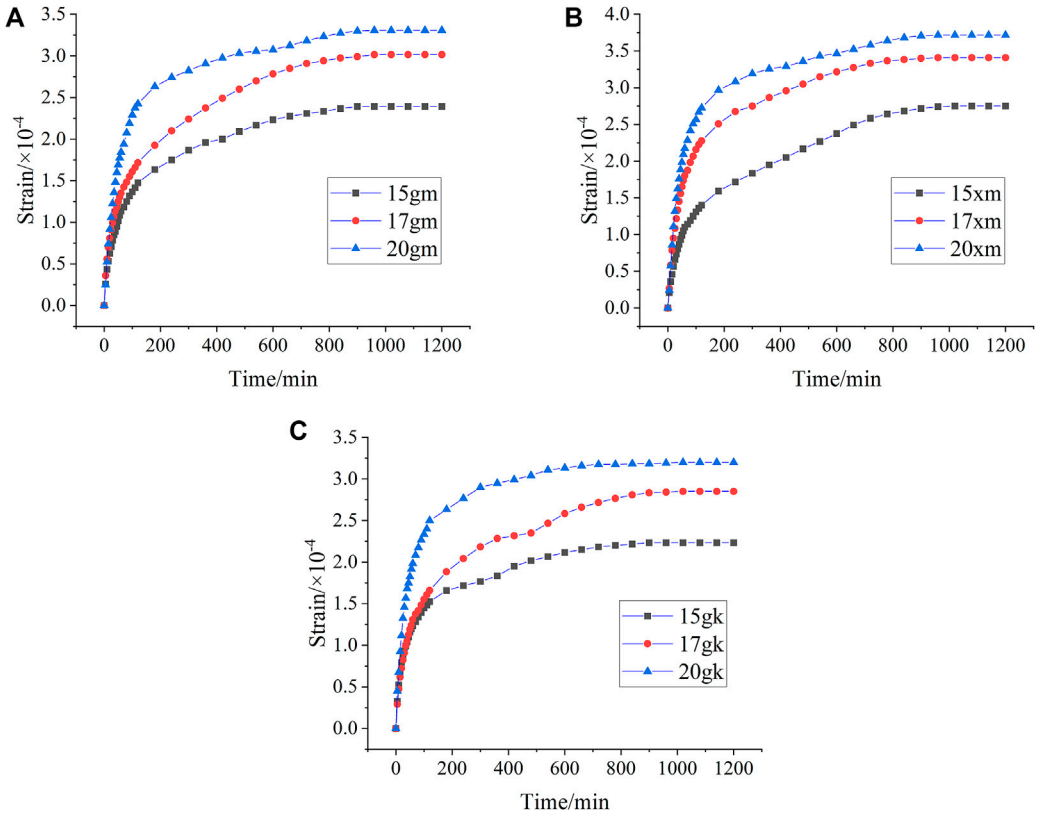

FIGURE 6
Relationship between the temperature shrinkage strain and time (grading type unchanged): **(A)** gm; **(B)** xm; and **(C)** gk.

180°min. Furthermore, when the lime–fly ash content was in a specific range, the xm-grade had the largest temperature shrinkage coefficient, followed by the gm-grade and gk-grade. Therefore, the suspended dense gradation should avoid a semi-rigid base layer.

The temperature shrinkage strain of the temperature shrinkage strain-stabilized macadam was also affected by the lime–fly ash content. Figure 6 shows the variations of the temperature shrinkage strain of different lime–fly ash contents with time. It is noticeable that the temperature shrinkage strain varies with time and exhibits similar trends with that of the internal temperature of the specimen. When the gradation type is fixed, the lower the lime–fly ash content, the smaller the temperature shrinkage strain of the lime–fly ash stabilized macadam is. For example, when the time is increased to 600°min, the strains for the lime–fly ash content of 15%, 17%, and 20% were 2.23×10^{-4}, 2.78×10^{-4}, and 3.08×10^{-4}, respectively, reflecting that the lime–fly ash content had the adverse impact on the base layer. Therefore, the content of lime–fly ash should be approximately reduced to control the temperature shrinkage strain of the base layer.

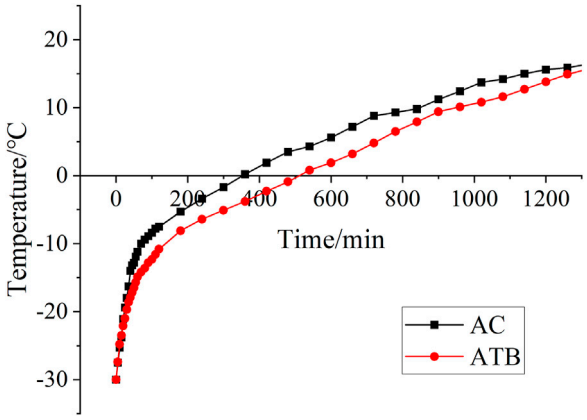

FIGURE 7
Relationship between the internal temperature and time of the asphalt mixture.

3.1.2 Asphalt mixture

The internal temperature of the asphalt mixture varies with time exhibits, as shown in Figure 7. It is evident from

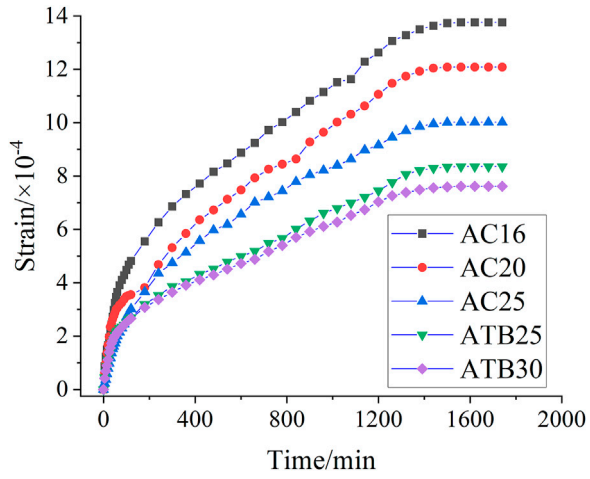

FIGURE 8
Relationship between the temperature shrinkage strain and time of the asphalt mixture.

Figure 7 that the internal temperature of the asphalt mixture increased with time. The internal temperature of the AC asphalt mixture is higher than that of the ATB asphalt mixture. For example, when the time increased to 420 min, the internal temperatures of AC and ATB asphalt mixtures were 1.9°C and −2.3°C, respectively. Moreover, the internal temperature increased sharply in the first 180 min and then increased slowly with time. For example, when the time increased from 0 min to 180 min, the internal temperature of AC and ATB asphalt mixtures increased from −30°C to −5.3°C and −8.1°C, while it increased from −5.3°C and −8.1°C to 18°C when the time-increasing amplitude increased from 180°min to 1,400°min.

The influence of the gradation type on the temperature shrinkage strain with time was analyzed (Figure 8). The temperature shrinkage strains increased gradually with the increase in time. In the first 180°min, the temperature shrinkage strain increased sharply and then slowly ranged from 180°min to 1,740°min. It is noticeable that the temperature shrinkage strain for the AC asphalt mixture was stable at about 1,440°min, whereas the ATB asphalt mixture was stable at about 1,620°min.

Moreover, it is evident that AC-16 had the largest temperature shrinkage strain for the surface layer, followed by AC-20 and AC-25. For example, when the time increased to 1,440 min (stable strain point), the temperature shrinkage strains of AC-16, AC-20, and AC-25 were 13.63×10^{-4}, 12.04×10^{-4}, and 9.95×10^{-4}, respectively, reflecting that the larger the nominal maximum aggregate size, the smaller the temperature shrinkage strain is. Therefore, to control the temperature shrinkage deformation of the surface layer, the nominal maximum aggregate size should be appropriately increased.

As for the flexible base course, the temperature shrinkage deformation of ATB-25 was greater than that of ATB-30. When the time increased to 1,620°min (stable strain point), the temperature shrinkage strains of ATB-25 and ATB-30 were 8.36×10^{-4} and 7.62×10^{-4}, respectively, indicating that the larger the nominal maximum aggregate size, the smaller the temperature shrinkage strain is. Thus, when the ATB gradation type was used as a flexible base course, priority should be given to that with a larger nominal maximum aggregate size to avoid temperature shrinkage deformation.

3.3 Effect of the structural combination on the temperature shrinkage coefficient

As previously discussed, the temperature rise method can be used to measure the temperature shrinkage coefficient for both the lime–fly ash-stabilized macadam and asphalt mixture. Thus, the temperature shrinkage coefficient of the composite structure was also measured by the temperature rise method in this work. The temperature range for the shrinkage test was −30°C–18°C, and the corresponding results are listed in Table 4 and Table 5.

The temperature shrinkage coefficient of the semi-rigid base asphalt pavement under different combinations was compared, as presented in Table 4. It is shown that the temperature shrinkage coefficient at the bottom of the composite structure was greater than that of the single lime–fly ash-stabilized macadam material. For example, when the content of lime–fly ash is 15%, the temperature shrinkage coefficient of that at the bottom of the 15 gm-AC-16 composite structure was 7.79×10^{-6}/°C, whereas the 15-gm base course was 4.98×10^{-6}/°C. This indicates that the surface layer promoted the temperature shrinkage of the base course in the process of temperature shrinkage of the composite structure. Moreover, the shrinkage increased differently when the types of composite structures were different. When the lime–fly ash contents were 15%, 17%, and 20%, the base course shrinkage growth rates were 20.3%–60.5%, 16.3%–46.7%, and 13.7%–46.2%, respectively.

Furthermore, the temperature shrinkage coefficient at the composite structure's bonding site was smaller than that of the single surface layer material. For example, at the bonding site of the 15-gm-AC-16 composite structure, the temperature shrinkage coefficient was 16.22, whereas the single surface layer was 28.65, reflecting that the temperature shrinkage of the bottom of the surface layer was inhibited by the base course. In addition, when the types of the base course were different, the shrinkage was different; thus, the inhibition effect of the base course on the bottom of the surface layer was different. When the lime–fly ash contents were 15%, 17%, and 20%, the reduction rates at the bonding site were 37.5%–44.6%, 35.7%–42.4%, and 28.0%–38.6%, respectively.

TABLE 4 Temperature shrinkage coefficient of the semi-rigid base asphalt pavement composite structure (×10^{-6}/°C).

Specimen type	Bottom of the base course			Joint			Top of the surface course		
	Combined structure	Base course	Growth rate (%)	Combined structure	Surface course	Reduction rate (%)	Combined structure	Surface course	Reduction rate (%)
15 gm-AC-16	7.79	4.98	54.2	16.22	28.65	43.4	20.52	28.65	28.4
15 gm-AC-20	7.21	4.98	44.8	14.19	25.17	43.6	18.39	25.17	27.0
15 gm-AC-25	6.95	4.98	39.5	12.71	20.87	39.1	16.93	20.87	18.9
15 xm-AC-16	9.19	5.73	60.5	17.68	28.65	38.3	21.74	28.65	24.1
15 xm-AC-20	8.62	5.73	50.5	14.77	25.17	41.3	19.17	25.17	23.9
15 xm-AC-25	7.89	5.73	37.7	13.05	20.87	37.5	17.71	20.87	15.1
15 gk-AC-16	7.14	4.65	53.4	16.61	28.65	42.0	18.54	28.65	35.3
15 gk-AC-20	6.17	4.65	32.6	13.96	25.17	44.6	16.59	25.17	34.1
15 gk-AC-25	5.60	4.65	20.3	12.76	20.87	38.9	15.34	20.87	26.5
17 gm-AC-16	9.22	6.28	46.7	18.28	28.65	36.2	20.94	28.65	26.9
17 gm-AC-20	8.75	6.28	39.2	14.95	25.17	40.6	19.11	25.17	24.1
17 gm-AC-25	7.37	6.28	17.3	13.36	20.87	36.0	17.60	20.87	15.6
17 xm-AC-16	10.05	7.10	41.6	17.84	28.65	37.7	20.76	28.65	27.5
17 xm-AC-20	9.19	7.10	29.5	15.55	25.17	38.2	19.61	25.17	22.1
17 xm-AC-25	8.26	7.10	16.3	13.28	20.87	36.4	17.11	20.87	18.0
17 gk-AC-16	8.67	5.94	46.1	16.77	28.65	41.5	19.71	28.65	31.2
17 gk-AC-20	8.05	5.94	35.5	14.51	25.17	42.4	18.36	25.17	27.1
17 gk-AC-25	7.40	5.94	24.6	13.41	20.87	35.7	16.98	20.87	18.6
20 gm-AC-16	10.08	6.89	46.2	18.52	28.65	35.4	21.35	28.65	25.5
20 gm-AC-20	9.53	6.89	38.3	15.47	25.17	38.6	20.03	25.17	20.4
20 gm-AC-25	8.23	6.89	19.4	13.88	20.87	33.5	18.36	20.87	12.0
20 xm-AC-16	10.68	7.74	37.9	19.30	28.65	32.6	22.16	28.65	22.6
20 xm-AC-20	10.00	7.74	29.1	16.46	25.17	34.6	20.42	25.17	18.9
20 xm-AC-25	9.06	7.74	17.0	15.03	20.87	28.0	18.57	20.87	11.0
20 gk-AC-16	9.66	6.67	44.9	18.10	28.65	36.8	20.96	28.65	26.8
20 gk-AC-20	8.39	6.67	25.8	15.76	25.17	37.4	19.61	25.17	22.1
20 gk-AC-25	7.58	6.67	13.7	14.61	20.87	30.0	18.02	20.87	13.6

Moreover, the temperature shrinkage coefficient of that at the top of the surface layer of the composite structure was smaller than that of the single surface layer material. This indicates that the temperature shrinkage at the top of the surface layer was also inhibited by the base course. However, the inhibition effect of the base course on the top of the surface layer was smaller than that at the bonding site.

The temperature shrinkage coefficient of the flexible base asphalt pavement composite structure is listed in Table 5. It can be seen from Table 5 that the temperature shrinkage coefficient of ATB asphalt mixtures in the composite structure was more significant than single ATB material. The growth rate of the temperature shrinkage coefficient was 3.6%–15.0%, reflecting that the shrinkage of the ATB base course in the composite structure was promoted by the surface layer.

Furthermore, the temperature shrinkage coefficient at the bottom of the surface layer was smaller than that of the single

TABLE 5 Temperature shrinkage coefficient of the flexible base asphalt pavement composite structure (×10^{-6}/°C).

Specimen type	Bottom of the base course			Joint			Top of the surface course		
	Combined structure	Base course	Growth rate (%)	Combined structure	Surface course	Reduction rate (%)	Combined structure	Surface course	Reduction rate (%)
ATB-25–AC-16	19.19	17.41	10.2	22.37	28.65	21.9	24.51	28.65	14.5
ATB-25–AC-20	18.67	17.41	7.2	21.04	25.17	16.4	22.27	25.17	11.6
ATB-25–AC-25	18.05	17.41	3.6	19.14	20.87	8.3	20.00	20.87	4.2
ATB-30–AC-16	18.26	15.87	15.0	21.51	28.65	24.9	22.97	28.65	19.8
ATB-30–AC-20	17.19	15.87	8.3	20.21	25.17	19.7	21.64	25.17	14.0
ATB-30–AC-25	16.88	15.87	6.3	18.59	20.87	10.9	18.91	20.87	9.4

ATB material, with a growth rate of 8.3%–24.9%. Therefore, the temperature shrinkage at the bonding site was inhibited by the base course, thus reducing the temperature shrinkage at the bonding site.

Moreover, the temperature shrinkage coefficient at the top of the surface layer was smaller than that of the single ATB material. The reduction rate was 4.2%–19.8%, indicating that the temperature shrinkage at the top of the surface layer in the composite structure was also inhibited by the base course. Meanwhile, the inhibition effect of the base course on the top of the surface layer was smaller than that at the bottom of the surface layer, that is, the closer to the base course, the greater is the inhibition effect on the temperature shrinkage of the surface layer.

Compared with the semi-rigid base asphalt pavement composite structure, the surface layer exerted an approximately small promotion effect on the base course in the flexible base asphalt pavement composite structure. Meanwhile, the inhibition effect of the base course on the surface layer was weak. This is because the temperature shrinkage coefficient of the ATB flexible base was larger than that of the semi-rigid base. The difference between the ATB base and the AC surface layer was small. Thus, after being combined with the asphalt surface layer, the interaction between the ATB base and AC surface layer was relatively small.

4 Conclusion

This work first discussed the temperature rise method to measure the temperature shrinkage coefficient of the lime–fly ash-stabilized macadam and asphalt mixture. Then, the temperature shrinkage coefficients of the semi-rigid base, flexible base, and surface layer were measured. The effect of gradation types and the lime–fly ash content on the temperature shrinkage coefficient was studied. Moreover, the temperature shrinkage coefficients of composite structures at different positions were measured. The mutual influence between the surface layer and base course in the process of shrinkage was analyzed. The following are the main conclusions from this study:

- The average temperature shrinkage coefficients measured by temperature rise and drop methods were not significantly different. Therefore, the temperature rise method can measure the temperature shrinkage coefficient.
- Based on the temperature shrinkage coefficient results obtained by the temperature rise method, it can be found that suspended dense gradation has the largest temperature shrinkage. Thus, suspended dense gradation should be avoided in the base course. Meanwhile, the temperature shrinkage strain of the lime–fly ash-stabilized macadam increased with an increasing lime–fly ash content. Therefore, the lime–fly ash content should be approximately reduced.
- The nominal maximum aggregate size affects the temperature shrinkage strain of both AC and ATB asphalt mixtures. The larger the nominal maximum aggregate size, the smaller the temperature shrinkage strain is. To avoid temperature shrinkage deformation, AC and ATB asphalt mixtures with a larger nominal maximum aggregate size should be given priority.

- The temperature shrinkage of the base course was promoted by the surface layer, while the surface layer was inhibited by the base course. Compared with the semi-rigid base asphalt pavement composite structure, the promotion and inhibition effects between the ATB base course and AC surface layer were relatively small.

Data availability statement

The original contributions presented in the study are included in the article/Supplementary Material; further inquiries can be directed to the corresponding author.

Author contributions

CJ: methodology and formal analysis; LZ: supervision; ZZ: writing–review and editing; HX and CJ: resources and validation; LZ: formal analysis.

Funding

This work was supported by the National Natural Science Foundation of China (grant number 52108410) and the China Postdoctoral Science Foundation (grant numbers 2022T150432 and 2021M702260).

Conflict of interest

The authors declare that the research was conducted in the absence of any commercial or financial relationships that could be construed as a potential conflict of interest.

Publisher's note

All claims expressed in this article are solely those of the authors and do not necessarily represent those of their affiliated organizations, or those of the publisher, the editors, and the reviewers. Any product that may be evaluated in this article, or claim that may be made by its manufacturer, is not guaranteed or endorsed by the publisher.

References

Akentuna, M., Kim, S. S., Nazzal, M., Abbas, A. R., and Arefin, M. S. (2016). Study of the thermal stress development of asphalt mixtures using the Asphalt Concrete Cracking Device (ACCD). *Constr. Build. Mater.* 114 (1), 416–422. doi:10.1016/j.conbuildmat.2016.03.207

Boucart, E., Konrad, J. M., and Pigeon, M. (2005). Simulation of thermal shrinkage at low temperature and of transverse cracking of a high performance recycled pavement. *Mat. Struct.* 38 (275), 127–136. doi:10.1007/bf02480585

Chu, I., Kwon, S. H., Amin, M. N., and Kim, J. K. (2012). Estimation of temperature effects on autogenous shrinkage of concrete by a new prediction model. *Constr. Build. Mater.* 35, 171–182. doi:10.1016/j.conbuildmat.2012.03.005

Coetzee, N. F., and Monismith, C. L. "Analytical study of minimization of reflection cracking in asphalt concrete overlays by use of a rubber-asphalt interlayer," in Proceedings of the 58th Annual Meeting of the Transportation Research Board, Washington, DC, USA, January 1979.

Fallah, S., and Khodaii, A. (2015). Reinforcing overlay to reduce reflection cracking; an experimental investigation. *Geotext. Geomembranes* 43 (3), 216–227. doi:10.1016/j.geotexmem.2015.03.002

Feng, D. C., and Song, Y. (2007). Study on test and evaluation method of asphalt pavement interlayer bonding state. *J. Harbin Inst. Technol.* (04), 627–631.

Hernando, D., and Val, M. D. (2016). Guidelines for the design of semi-rigid long-life pavements. *Int. J. Pavement Res. Technol.* 9 (2), 121–127. doi:10.1016/j.ijprt.2016.03.003

Jtg E51 (2009). *Test methods of materials stabilized with inorganic binders for highway engineering*. Beijing, China: China Communication Press.

Jtg F40 (2004). *JTG F40-2004 Technical specification for construction of highway asphalt pavement*. Beijing, China: China Communication Press.

Jtj 034 (2000). *JTJ 034-2000 Technical specifications for construction of highway roadbases*. Beijing, China: China Communication Press.

Kazimierowicz-Frankowska, K. (2016). Influence of cracks on the lifetime of semi-rigid pavements. *Archives Hydro-Engineering Environ. Mech.* 63 (2-3), 83–100. doi:10.1515/heem-2016-0006

Li, W., Lang, L., Lin, Z. Y., Wang, Z. H., and Zhang, F. G. (2017). Characteristics of dry shrinkage and temperature shrinkage of cement-stabilized steel slag. *Constr. Build. Mater.* 134, 540–548. doi:10.1016/j.conbuildmat.2016.12.214

Ma, L. K., Li, M., Pang, J. S., and Huang, C. W. (2019). Evaluation of transverse cracks for semi-rigid asphalt pavements using deflection basin parameters. *Transp. Res. Rec.* 2673 (2), 358–367. doi:10.1177/0361198119826075

Ma, X. Q., Xue, X., and Cheng, X. P. (June 2013). "Shrinkage performance of lime-fly ash stabilized crushed stone," in Proceedings of the International Conference on Materials, Transportation and Environmental Engineering (CMTEE 2013), Taichung, TAIWAN.

Szwed, A., and Kamińska, I. (2015). Mitigation of low-temperature cracking in asphalt pavement by selection of material stiffness. *Procedia Eng.* 111, 748–755. doi:10.1016/j.proeng.2015.07.141

Tian, D. T., and Dai, H. M. (1987). *Frost damage of roads and bridges and its prevention*. Beijing, China: China Communication Press.

Tian, L. (2010). Research on anti-cracking characteristics of frame-densed cement stabilized graded crushed stone. Harbin Institute of Technology. Harbin, China, dissertation.

Wang, X. Y., Li, K., Zhong, Y., Xu, Q., and Li, C. Z. (2018). XFEM simulation of reflective crack in asphalt pavement structure under cyclic temperature. *Constr. Build. Mater.* 189, 1035–1044. doi:10.1016/j.conbuildmat.2018.08.202

Yang, B., Wang, L. H., Dai, C. Y., and Destech Publicat, I. (December 2013). "Influences on thermal stress of pavement slab caused by crack or cutting crack in semi-rigid base," in Proceedings of the International Conference on Transportation (ICTR), Xianning, PEOPLES R CHINA. Wuhan, China,

Yang, W. D. (2004). Study on Shrinkage Properties of semi-rigid base materials. Chang'an University. master's thesis. Xi'an, China.

Yu, X. J. (2016). Analysis of influence factors on the adhesion performance of asphalt pavement in Expressway. *Jiangxi Build. Mater.* (10), 167–170.

Zang, G. S., Sun, L. J., Chen, Z., and Li, L. (2018). A nondestructive evaluation method for semi-rigid base cracking condition of asphalt pavement. *Constr. Build. Mater.* 162, 892–897. doi:10.1016/j.conbuildmat.2017.12.157

Zhai, F., Feng, Y., Li, Y., Xie, Y., Ge, J., Wang, H., et al. (2021). 4D printed untethered self-propelling soft robot with tactile perception: Rolling, racing, and exploring. *Matter* 4, 3313–3326. doi:10.1016/j.matt.2021.08.014

Zhai, F., Feng, Y., Zhou, K., Wang, L., Zheng, Z., and Feng, W. (2018). Graphene-based chiral liquid crystal materials for optical applications. *J. Mat. Chem. C Mat.* 7, 2146–2171. doi:10.1039/c8tc04947e